Nanoscale

PAPER

View Article Online
View Journal | View Issue

Cite this: *Nanoscale*, 2019, **11**, 11617

A biomimetic magnetosome: formation of iron oxide within carboxylic acid terminated polymersomes†

Jennifer Bain,‡ Christopher J. Legge,‡ Deborah L. Beattie,‡ Annie Sahota,‡ Catherine Dirks,‡ Joseph R. Lovett and Sarah S. Staniland *

Bioinspired macromolecules can aid nucleation and crystallisation of minerals by mirroring processes observed in nature. Specifically, the iron oxide magnetite (Fe_3O_4) is produced in a dedicated liposome (called a magnetosome) within magnetic bacteria. This process is controlled by a suite of proteins embedded within the liposome membrane. In this study we look to synthetically mimic both the liposome and nucleation proteins embedded within it using preferential orientation polymer design. Amphiphilic block co-polymers self-assemble into vesicles (polymersomes) and have been used to successfully mimic liposomes. Carboxylic acid residue-rich motifs are common place in biomineralisation nucleating proteins and several magnetosome membrane specific (Mms) proteins (namely Mms6) have a specific carboxylic acid motifs that are found to bind both ferrous and ferric iron ions and nucleate the formation of magnetite. Here we use a combination of 2 diblock co-polymers: Both have the hydrophobic 2-hydroxypropyl methacrylate (PHPMA) block with either a poly(ethylene glycol) (PEG) block or a carboxylic acid terminated poly(2-methacryloyloxyethyl phosphorylcholine) (PMPC) block. These copolymers ((PEG_{113}-$PHPMA_{400}$) and ($PMPC_{28}$-$PHPMA_{400}$) respectively) self-assemble *in situ* to form polymersomes, with PEG_{113}-$PHPMA_{400}$ displaying favourably on the outer surface and $PMPC_{28}$-$PHPMA_{400}$ on the inner lumen, exposing numerous acidic iron binding carboxylates on the inner membrane. This is a polymersome mimic of a magnetosome (PMM_{28}) containing interior nucleation sites. The resulting PMM_{28} were found to be 246 ± 137 nm in size. When the PMM_{28} were subjected to electroporation (5 pulses at 750 V) in an iron solution, iron ions were transported into the PMM_{28} polymersome core where magnetic iron-oxide was crystallised to fill the core; mimicking a magnetosome. Furthermore it has been shown that PMM_{28} magnetopolymersomes ($PMM_{28}Fe$) exhibit a 6 °C temperature increase during *in vitro* magnetic hyperthermia yielding an intrinsic loss power (ILP) of 3.7 $nHm^2\ kg^{-1}$. Such values are comparable to commercially available nanoparticles, but, offer the added potential for further tuning and functionalisation with respect to drug delivery.

Received 16th January 2019,
Accepted 11th April 2019

DOI: 10.1039/c9nr00498j

rsc.li/nanoscale

Introduction

Biological iron oxide precipitation

The presence of iron oxide particles has been found in various species of birds and dolphins.[1,2] While the true function and mechanism of action of these particles has never been properly explained, it is widely believed that in most cases they play an essential role in navigation by acting as "internal compasses". The formation of such particles is the result of biomineralization. Biomineralization involves precipitation of an inorganic material within or around living organisms.[3] These minerals typically fulfil a specific function, such as forming a protective shell or a structural skeleton.[2] Biominerals often possess highly controlled size, shape and crystal structure compared to the equivalent synthetic materials.[4] This level of structural control can be difficult to achieve in the laboratory because most biomineralization processes are governed by a complex suite of proteins, usually embedded within templating membranes.[4]

Precipitation of magnetite in magnetotactic bacteria

Magnetotactic bacteria are the smallest organisms that are known to perform biomineralization. Most strains precipitate pure magnetite nanoparticles (MNPs) within internally formed vesicular organelles, known as "magnetosomes". Precise mag-

Department of Chemistry, University of Sheffield, Sheffield, S3 7HF, UK.
E-mail: S.S.Staniland@sheffield.ac.uk

†Electronic supplementary information (ESI) available. See DOI: 10.1039/c9nr00498j

‡These authors contributed equally to this work.

netite crystallisation within the magnetosome is controlled by various proteins that are responsible for specific stages of the overall process, from recruitment of soluble iron species into the magnetosome lumen through transmembrane iron-transporter proteins[5,6] to its nucleation and subsequent controlled crystal growth. The resulting magnetite nanoparticles are well known for their precise mono-dispersed size and morphology.

Nucleation biomineralisation proteins for iron oxide precipitation

Some common mechanistic feature are exhibited across a range of biomineralisation processes. One such example is the concentration of metals ion and nucleation of the mineral on a nucleation protein. The common features of these proteins are the large proportion of carboxylic acid residues[7] available to bind and accumulate metal cations (such as iron or calcium). For example, approximately a third of all the amino acid residues in the bone mineralising protein osteopontin are the two carboxylic acids aspartic (D) or glutamic (E) acid.[8] The integral nature these amino acids have on biomineralisation has further been elegantly demonstrated with chiral glutamic and aspartic acids producing chiral vaterite ($CaCO_3$) minerals.[9] Magnetosomes also contain acidic nucleation proteins. Mms6 is a small acidic magnetosome membrane specific (Mms) protein 6 kDa in size located on the magnetosome interior. It was found strongly bound to the magnetite crystal when the magnetosome membrane was removed,[10] and the purified protein has been shown to control magnetite particle formation *in vitro*.[10,11] The C-terminus of the protein (predicted to be on the interior and thus exposed to the forming magnetite) has a large number of acidic residues believed to play a key role as a nucleation site for the biomineralization of magnetite.[12–15] A DEEVE motif, has been shown to change conformation on binding ferrous ion[12,16] while ferric ion have been shown to bind readily and less specifically to multiple acidic residues on the C-terminus.[12,14,15] Like many other nucleation proteins, Mms6 protein is known to aggregate to display a surface of carboxylate groups on the inner lumen of the magnetosome membrane that promotes magnetite nucleation.[12] A similar acidic region is a common feature of several Mms proteins in the magnetosome including Mms7 and MmsF, strongly suggesting that magnetite biomineralization is aided by carboxylic acid-functionalization on the inner lumen on the vesicle.[11,17,18]

Bioinspired iron oxide precipitation in polymersomes

Applications of magnetopolymersomes. The incorporation of MNPs into vesicles can introduce multi-functionality into established vesicular drug delivery systems undergoing clinical trials worldwide.[19–21] Functionalisation of these vesicles with MNPs can allow steering with a magnetic field enabling drug targeting. Further, simultaneous imaging during drug delivery through magnetic resonance imaging (MRI) can be achieved, allowing for *in situ* monitoring of therapeutic delivery. Furthermore, and perhaps most extensively researched, MNPs can provide alternative or additional hyperthermic heating therapies. Application of an alternating magnetic field can cause localised heating of tissue known as magnetic hyperthermia, destroying diseased tissue or sensitising the local area to further therapeutics. The ability of MNP materials to heat can be quantified by the specific absorption rates (SAR), which is the heating power. The measure of heating power normalised to the magnetic field and frequency is the intrinsic loss power (ILP) parameter. ILP values between 1.6 & 5 $nHm^2\ kg^{-1}$ have been extensively reported for various synthetic magnetopolymersomes and are shown to be functional for hyperthermic therapies.[22]

However, magnetosomes have a much larger magnetic heat loss than comparatively sized synthetic magnetite nanoparticles at lower fields[23] with SAR from 600 W g^{-1} to 960 W g^{-1} reported (depending on the magnetic field strength and frequency) and with a the very high ILP of 23.4 $nHm^2\ kg^{-1}$.[24,25]

Control of MNP precipitation within a vesicle has a direct effect on the heating achieved during *in vivo* hyperthermic application[26] and bioinspired routes to precipitation offer the potential to tightly control precipitation leading to increased levels of monodispersity which could vastly improve current nanomedical materials.[27,28]

Creating a polymersome nanoreactor. A synthetic vesicle can provide a perfect analogue to the biologically formed magnetosome. There are many examples of polymer vesicles (or polymersomes) being used to mimic liposomes. Ideally, we would mimic a magnetosome using a polymersome with a basic core as a nanoreactor for magnetite precipitation by importing iron ions across the membrane into the alkaline core. However, our previous attempts to use a diblock polymersome to mimic a magnetosome have resulted in MNPs precipitated within the polymer membrane[29] and a triblock polymersome yielded MNPs again mainly within the membrane with some precipitation within the core.[30]

Iron transport *via* electroporation. We and others have previously shown that the application of an electric field can cause a polymersome membrane to porate (form pores) and enable synthetic intravesicular diffusion, a process known as electroporation.[23,31–33] Electroporation is a technique widely used in biology for the transformation of DNA into cells by electrically permeablising a cell membrane through application of a pre-determined voltage.[31,32,34,35] The mechanism by which the membrane is permeated has been widely explored, but as yet has not been fully understood.[33,36] Electroporation is the method we exploit to import soluble iron ions into the polymersomes in our previous studies resulting in iron oxide precipitation mainly within the membrane.[29,30] We conclude that without specific internal nucleation sites, iron oxide will precipitate indiscriminately in an uncontrolled fashion.

Mimicking membrane/protein surface of the magnetosome. The inner lumen of the magnetosome membrane contains a range of biomineralisation proteins. Importantly, carboxylic acid rich nucleation proteins such as Mms6, which display a negatively charged surface for iron ion binding to nucleate magnetite formation. In this work we have advanced our pre-

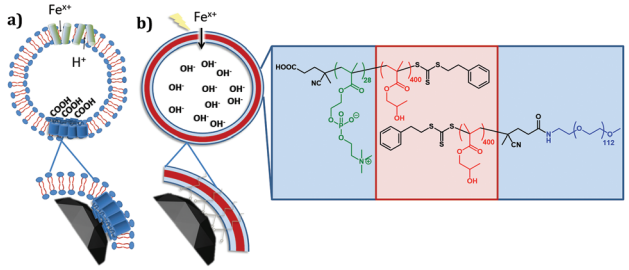

Fig. 1 Schematic of natural and synthetic vesicle membranes (blue = hydrophilic membrane leaflet, red = hydrophobic membrane leaflet) representing, (a) the bacterial magnetosome in which iron is recruited into the core of the magnetosome using iron transporters, which also acts an antiporter pumping out internal protons. The efflux of protons causes a pH increase resulting in the precipitation the magnetite crystal. The magnetite nucleation protein Mms6 (inset bottom left) which accumulates iron ions on the acidic amino acids on the inner lumen of the magnetosome. (b) Chemical composition of PEG-PHPMA and PMPC-PHPMA polymer which represent the hydrophilic (blue) and hydrophobic (red) leaflets of the vesicles, which features a carboxylic acid group on the PMPC monomer to mimic the iron ion binding/mineral nucleating sites of the Mms6 protein. The lighting represents electroporation to mimic the protein iron transporter, while the insert shows how the acidic end groups on PMPC mimic Mms6.

vious polymersomes by designing and creating a new di-block co-polymersome that will better mimic the magnetosome. Specifically, we have designed one copolymer to include a short hydrophilic block that displays carboxylate groups, while the other will instead include a longer neutral block. Due to the curvature of the polymersome we predict that steric factors will orientate the shorter acidic copolymer on the interior, displaying it's acidic groups on the inner surface of the polymersome, while the bulkier copolymer will preferentially orientate on the exterior. The polymer system designed and presented in this work should now enable more preferential and controlled particle formation inside the polymersome (as opposed to within the membrane) by mimicking the action of nucleating proteins on the inner membrane (Fig. 1).

PEG-PHPMA/PMPC-PHPMA polymersomes

Poly(2-(methacryloyloxy)ethyl phosphorylcholine)-poly(2-hydroxypropyl methacrylate) (PMPC-PHPMA) is a vesicle-forming diblock copolymer that has a terminal carboxylic acid group situated on the hydrophilic PMPC block. In principle, addition of such groups should mimic the iron ion binding sites found in the Mms6 protein (mimicked by the COOH end group) within the magnetosomes liposome (lipid mimicked by the phosphorylcholine). It should be noted that carboxybetaine zwitterionic groups similar to phosphorylcholine have been shown to not interact with calcite mineralisation, to the extent they are not incorporated into calcite mineral whereas COOH groups alone do, so interaction with the negative charge on zwitterionic phosphorylcholine is improbable.[37] Moreover, preferential location of these carboxylic acid liposome-mimicking groups on the polymersome inner leaflet should create a synthetic mimic of a nucleation protein within the magnetosome membrane (Fig. 1). In practice, this is achieved using a binary mixture of the PMPC-PHPMA chains with a second diblock copolymer, poly(ethylene glycol)-poly(2-hydroxypropyl methacrylate) (PEG-PHPMA). The two weakly hydrophobic PHPMA blocks have the same mean degree of polymerisation and co-assemble to form the vesicle membrane. However, the PMPC and PEG chains are thermodynamically incompatible.[38] Hence microphase separation occurs across the vesicle membrane, with the shorter PMPC block being preferentially expressed at the inner leaflet, while the longer PEG block is located mainly at the outer leaflet.

It is well known that amphiphilic diblock copolymers undergo spontaneous self-assembly in water.[39–41] Traditionally diblock copolymers are prepared in a solvent with ideal solubility for both blocks before being transferred into water.[42] Such copolymers can assemble into spheres, worms or vesicles depending on the relative volume fractions of each block.[41,43] More recently several groups have utilised polymerisation-induced self-assembly (PISA) to prepare nano-objects *in situ*.[44–46] More specifically, a soluble homopolymer is chain-extended with a monomer which when polymerised forms the insoluble core-forming block. For example, a poly(ethylene glycol) macromolecular chain transfer agent (PEG macro-CTA) has been prepared *via* end-group derivatization and subsequently chain-extended with HPMA *via* reversible addition–fragmentation chain transfer (RAFT) aqueous dispersion polymerization.[45] By varying the degree of polymerization (DP) of the core-forming PHPMA block and also the copolymer concentration, pure spheres, worms or polymersomes could be prepared in concentrated aqueous solution. Similarly, chain-extending a PMPC macro-CTA with HPMA enabled the synthesis of a similar series of PMPC-PHPMA nano-objects.[47] In both cases, PISA syntheses had to be conducted at relatively high copolymer concentration (20–25% w/w) in order to produce a pure polymersome phase. According to Gonzato and co-workers,[48] using a binary mixture comprising a short macro-CTA and a long macro-CTA should produce low-polydispersity polymersomes, whereby the short macro-CTA chains are mainly located within the inner lumen, while the long macro-CTA chains are preferentially expressed at the outer surface of the polymersomes.[45] In the present work, we have explored the use of a relatively long PEG macro-CTA in conjunction with a relatively short PMPC macro-CTA to polymerize HPMA *via* RAFT aqueous dispersion polymerization (Fig. 2). Microphase separation of these two steric stabilizer blocks across the membrane was anticipated, not least because Blanazs and co-workers have shown that PEG and PMPC homopolymers are enthalpically incompatible.[38] Moreover, judicious selection of a carboxylic acid-functionalized RAFT agent for the synthesis of the PMPC macro-CTA enables the construction of polymersomes in which the acid end-groups on this stabilizer block are mainly located within the lumen.[49] Thus such polymersomes mimic the structure of naturally-occurring bacterial magnetosomes containing the Mms6 protein. Following the work of Chambon *et al.*,[50] such poly-

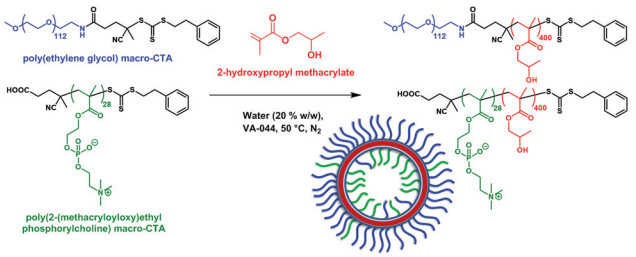

Fig. 2 Poly(ethylene glycol)-poly(2-hydroxypropyl methacrylate)/poly (2-(methacryloyloxy)ethyl phosphorylcholine)-poly(2-hydroxypropyl methacrylate) (PEG + PMPC)-PHPMA polymersomes are prepared by chain extension of a binary mixture of PEG_{113} and $PMPC_{28}$ macro-CTAs *via* reversible addition–fragmentation chain transfer (RAFT) aqueous dispersion polymerisation of 2-hydroxypropyl methacrylate (HPMA).[45]

mersomes can be covalently stabilized by addition of a bifunctional cross-linker at high HPMA conversions (>99%). PEG-PHPMA/PMPC-PHPMA vesicles assemble as part of the polymer synthesis process. Therefore, it is not possible to encapsulate base during rehydration. Instead, we report the novel methodology of soaking pre-formed polymersomes in NaOH.

Using this di-block system we have designed and are able to produce synthetic polymersomes that mimic magnetosomes (PMM_{28}).

Materials and methods

Materials

All solutions used were degassed and sparged with N_2 prior to use and all experiments were carried out under an inert atmosphere to minimise iron oxidation. 2-(Methacryloyloxy)ethyl phosphorylcholine (MPC; >99%) was donated by Biocompatibles Ltd (Farnham, UK). 2-Hydroxypropyl methacrylate (HPMA) was purchased from Alfa Aesar, 2,2′-azobis[2-(2-imidazolin-2-yl)propane] dihydro-chloride (VA-044) was purchased from Wako Pure Chemical Industries (Japan), ethylene glycol dimethacrylate (EGDMA) was purchased from Sigma Aldrich. All the above were used as received. PEG_{113} macro-CTA was prepared as reported elsewhere.[45] All other chemicals were purchased from Sigma Aldrich, unless otherwise stated.

Polymersome synthesis

PMPC macro-CTA was prepared as reported elsewhere.[47] A typical protocol for the synthesis of PMM_{28} polymersomes (self-assemblies of 70% PEG_{113} $PHPMA_{400}$ and 30% $PMPC_{28}PHPMA_{400}$) is as follows: PEG_{113} macro-CTA (0.0735 g, 1.4×10^{-5} mol), $PMPC_{28}$ macro-CTA (0.0516 g, 6.0×10^{-6} mol); vA-044 initiator (0.00187 g, 6.7×10^{-6} mol), ([combined CTA]/[VA-044] molar ratio = 3.0) and HPMA monomer (1.12 g, 8.0×10^{-3} mol, target DP = 400) were dissolved in deoxygenated water to generate a 20% w/w solution. The pH of the solution was adjusted to pH 6.8 using 0.1 M NaOH. This solution was then purged with nitrogen for 30 minutes. The flask was sealed using a rubber septum and immersed in an oil bath at 50 °C. When the polymerisation had proceeded for 4 hours, the reaction was quenched by exposure to air and cooling to 20 °C. Cross-linked polymersomes, were synthesised as described above, but, after 4 hours degassed EGDMA (0.158 g, 8×10^{-4} mol) was added under N_2, and left to stir for 12 hours at 50 °C.

^{1}H NMR

^{1}H NMR was used to calculate conversion in the synthesis of 70% PEG_{113}-$PHPMA_{400}$, 30% $PMPC_{28}$-$PHPMA_{400}$ to form PMM_{28}. Spectra were acquired using a Bruker Avance III HD 400 spectrometer. Samples were prepared by dissolving 100 μL polymersomes solution in CD_3OD (3 mL).

Electroporation of polymersomes

PMM_{28} polymersomes were incubated in 10 mM NaOH, then cleaned up using a size exclusion chromatography (SEC) column. A 1 : 2 Fe(II) : Fe(III) stock iron solution was prepared by mixing 1 ml of 10 mM $FeCl_2{\cdot}4H_2O$ solution (0.019 g, 1.00×10^{-4} mol, 10 mL, dissolved in degassed water) with 2 ml of 10 mM $FeCl_3{\cdot}6H_2O$ solution (0.027 g, 1.00×10^{-4} mol, 10 mL, dissolved in degassed water). The PMM_{28} polymersomes with now basic cores were electroporated using a BioRad Micropulser™. 100 μL of basic PMM_{28} were incubated with 100 μL of mixed valence iron solution (in a 1 : 1 v/v ratio), before being electroporated at a maximum volume of 800 μl. 5 pulses were applied at a voltage of 750 V, to facilitate transport of the iron ion solution as previously published.[30] SEC Cleaned electroporated PMM_{28} were visualised unstained using TEM (Fig. 4).

Dynamic light scattering (DLS)

5 μl of the vesicle samples were diluted in 1 ml of MilliQ water before analysis in a disposable DLS cuvette using a scattering angle of 173° on a Zetasiazer Nano (Malvern Instruments). Samples were scanned three times at a standard temperature of 25 °C, with each scan having 10–14 runs; data were analysed using Malvern Zetasizer software.

Transmission electron microscopy (TEM)

Transmission electron microscopy (TEM) was used to visually assess the polymersomes size, shape and integrity pre and post electroporation. The size and location of the iron oxide precipitation associated with the vesicle was assessed post-electroporation and selected area electron diffraction was used to assess crystallinity of the iron oxide. 5 μl of the polymersome sample (diluted 1 : 1000% v/v) was applied to a carbon film grid and left to stand for approximately 1 minute, before blotting off excess liquid. Grids were then dried at ambient temperature. All post-electroporation samples were imaged unstained. Control samples assumed not to contain dense iron minerals were subsequently stained (0.75% uranyl formate) prior to imaging, before blotting off after a 12 seconds staining period. Samples were imaged using a Tecnai F20 and images processed using ImageJ.

Inductively coupled plasma emission spectrometry (ICP-ES)

Inductively coupled plasma emission spectrometry, (Specto-Ciros-Vision Inductively Coupled Plasma Optical Emission Spectrometer) was used to determine iron concentrations in the PMM_{28}Fe samples. ICP-ES samples were prepared for detection of iron concentration, by dissolving a known volume of magnetopolymersomes sample (100 μl) in aqua regia to a total volume of 5 ml (4 parts water to 1 part acid). The iron content was detected and measured against calibration standard of known concentrations.

Magnetic hyperthermia measurements

PMM_{28} magnetopolymersomes were analysed for their use as agents in magnetic hyperthermia, using a Nanotherics MagneTherm®. Measurements were taken using a 17 turn coil with a frequency of 636 kHz, an applied voltage of 19.0 V creating a current of 5.2 A across the coil. The field within the coil was calculated to be 7.2 kA m^{-1}. A grant recirculating water bath, maintained a constant base temperature of 10 °C around the coil. A 200 μl 1.0% w/v aqueous dispersion of PMM_{28}Fe polymersomes was made up to 1 ml with ultrapure water (0.11 mg ml^{-1} of iron) and the temperature measured in the alternating field over a period of 10 minutes, using a single channel fibre optic thermometer (Lambda Photometrics Ltd). Control measurements of the blank polymersomes of the same concentration in PBS solution were taken and subtracted from the PMM_{28}Fe data. The data was used to extract the SARs and ILP values, analysed using software from Resonant Circuits Limited, with consideration of all parameters that can skew the data.[51] The SAR and the ILP are defined by equations 1 & 2 below, where $\Delta T/\Delta t$ is the initial gradient of the change in temperature over time, c is the heat capacity of water, M_{Fe} is the mass of iron per ml, H is the magnetic field and f is the frequency of the alternating field.

$$\mathrm{SAR} = \frac{\Delta T}{\Delta t}\frac{c}{M_{\mathrm{Fe}}} \quad (1)$$

$$\mathrm{ILP} = \frac{\mathrm{SAR}}{H^2 f}. \quad (2)$$

Results and discussion

Polymersome synthesis

PMM_{28} were prepared by PISA *via* RAFT aqueous dispersion polymerisation of HPMA at pH 6.5 with a 70% : 30% ratio of PEG_{113}-$PHPMA_{400}$ to $PMPC_{28}$-$PHPMA_{400}$. ^{1}H NMR studies indicated high monomer conversions (>99%) after 4 hours at 50 °C, indicated by the loss of the vinyl group peaks at 5.5 ppm (ESI 1†). To obtain a high pH (basic) PMM_{28} core, PMM_{28} were soaked in NaOH to diffuse into the core. TEM confirms that this process did not affect the appearance of the vesicles. TEM imaging shows a mixture of spherical and elongated PMM_{28} vesicles with a relatively disperse size population (Fig. 3a) with the sizes being maintained in hydrated conditions when imaged using cryo-TEM (Fig. 3b). This is

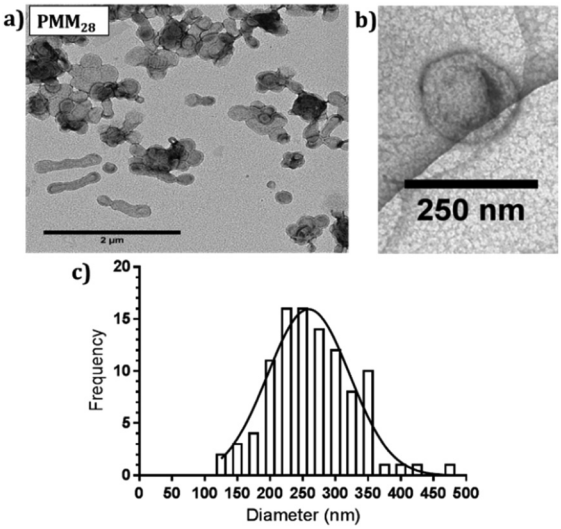

Fig. 3 (a) Negatively stained TEM images of PMM_{28} polymersomes, (b) cryo-TEM image of PMM_{28} to show hydrated size is consistent with (a). (c) TEM grainsizing of the polymersome sample.

reflected in grainsize analysis of the polymersomes, giving a high polydispersity of 224 ± 209 nm (Fig. 3c). The grainsizing analysis from the TEM images also correlates well with the DLS analysis, showing a stable size across the pH range from 2–10, maintaining an average vesicle diameter of 246 nm (ESI 2†). Zeta potential decreases as the pH is increased from 2–9 with the hydrophilic surface of polymersomes becoming negatively charged at pH's above 3.5 (ESI 2†), indicating that the vesicles will maintain a negatively charged surface through deprotonation of the carboxylic acid through each stage of the iron oxide precipitation experiment.

PMM_{28} iron oxide precipitation through electroporation to form PMM_{28}Fe

PMM_{28} with a basic core (through NaOH soaking) were added to a mixed valence iron salt solution (1 : 2, Fe(II) : Fe(III)) but no precipitation was observed. After several days only a small amount of precipitation of electron dense iron oxide on the outer membrane of polymersomes was observed but no or negligible internal iron oxide precipitation (ESI 3†), suggesting the membrane is impermeable to iron ions and only limited quantities of OH^- seep out after several days. Thus an iron ion transport mechanism is required such as electroporation.

Therefore, basic PMM_{28} were subjected to our previously published method of electroporation to import iron ions into the NaOH PMM_{28} core to induce iron oxide precipitation.[29,30] Here, we improve on our previous method, as PMM_{28} offers carboxylic acid iron nucleation sites inside the core which should promote more iron oxide inside the polymersome rather than in the membrane.

Electroporation of PMM_{28} basic polymersomes in an iron solution was successful, with the polymersomes showing distinct electron dense cores (attributed to precipitation of iron oxide) consistent across all the PMM_{28}Fe sample (Fig. 4) which

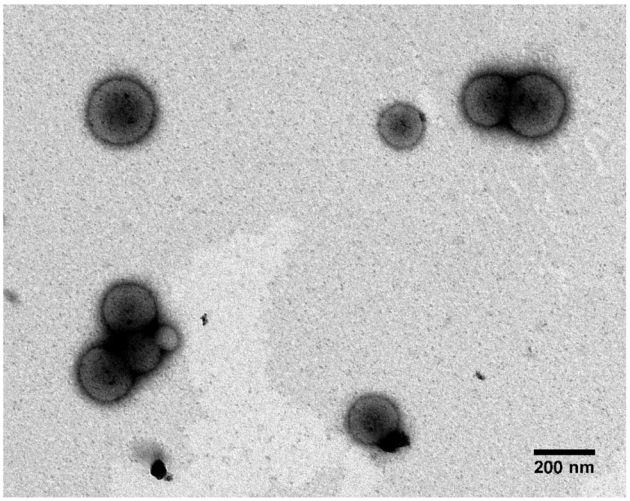

Fig. 4 Unstained TEM images of (a) $PMM_{28}Fe$. The PMM_{28} sample was soaked in NaOH (10 mM) before electroporation at 750 V (5 pulses) in the presence of excess $FeCl_2{\cdot}4H_2O$. The polymersomes show dark electron dense cores, attributed to the precipitation of magnetic iron oxide.

is not seen in the PMM_{28} prior to electroporation (compare Fig. 4 with ESI 3†).

The electroporated $PMM_{28}Fe$ are visibly more spherical uniformly across the whole population and are also smaller with a narrower size distribution (212 ± 79 nm). The filled cores appear to be made up of aggregates of smaller MNPs of iron oxide, with some discreet particles visible nearer the membrane as the density of iron oxide reduces radially from the centre (Fig. 5a). The size of these isolated particles was determined to 5.54 ± 0.55 nm (ESI 4†). Furthermore, the iron oxide-loaded polymersomes were found to be magnetic (attracted to a permanent magnet) and selected area electron diffraction confirms that the precipitation visible in the polymersome core was crystalline, indicating the iron oxide core is crystalline magnetite or maghemite (Fig. 5b). ICP elemental analysis gave

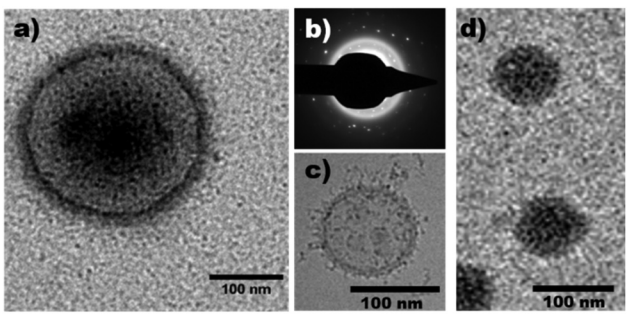

Fig. 5 (a) Unstained TEM image of electroporated $PMM_{28}Fe$ polymersomes showing precipitation on the outer leaflet of the polymersome as well as in the vesicle core. (b) A selected area electron diffraction image of the same electroporated polymersome confirming the presence of a crystalline substance within the polymersome. (c) Cryo-EM micrograph of PEO-PBD polymersomes from the first reported use of the electroporation method[29] and (d) show comparison of use of the electroporation method on PMOXA-DMS-MOXA tri-block polymersomes.[30]

27.5 μg ml^{-1} of Fe to 0.5 mg ml^{-1} of polymersomes giving approximately 5.5% iron content by weight in $PMM_{28}Fe$.

Comparison to other magnetopolymersomes

This is the first example of the precipitation of magnetic iron-oxide densely concentrated into the core of a polymersome (Fig. 5a). Our previous work utilising electroporation to produce magnetopolymersomes was conducted on poly(butadiene)-poly(ethylene oxide) (PBD-PEO) diblock co-polymersomes. PBD-PEO polymersome possess no functional nucleation sites and as a result the MNPs simply form in the membrane where the two reagents (iron ions and NaOH) meet in the pores opened by the electroporation process (Fig. 5c).[22] Similarly we have demonstrated electroporation can be used to produce magnetopolymersomes from Tri-block co-polymers by precipitate MNPs within an ABA Tri-block co-polymersome composed of PMOXA-PDMS-PMOXA (where PMOXA = poly(2-methyloxazoline) & PDMS = poly(dimethylsiloxane)) (Fig. 5d).[30] Again, there are no functional nucleation sites on this polymer and while we believe there may be more internal MNPs in this example (possibly due to the different structural configuration of pore formation for a tri-block under electroporation conditions), the size of particles formed in both these two previously reported examples is ~2.6 nm. This contrasts with this current study which shows a two-fold increase in the particle size (5.5 nm) and the overall quantity and quality of precipitation within the $PMM_{28}Fe$ core. ICP elemental analysis shows an approximate 5-fold minimal increase in quantity of elemental iron compared with both the tri-block and di-block.[29,30] This strongly indicates that the COOH groups promote more internal nucleation of larger MNPs.

Effect of crosslinking PMM_{28}

There is a clear electron dense "halo" on the outer leaflet of the polymersomes. The chromatography clean-up removes all un-associated iron oxide precipitate, showing the iron oxide halo to be strongly associated with the vesicles surface (Fig. 4 & 5a). This could be evidence for the presence of deprotonated carboxylic acid groups on the outer surface of the vesicle, nucleating and forming iron-oxides on the exterior. Ideally the acidic shorter polymer chains in the PMPC block would exclusively orientate to the inner lumen of the polymersome, however, a small amount of carboxylic acid groups may misorientate at the formation stage or flip to the exterior once formed. Crosslinking could reduce polymer flipping post-formation.

Ethylene glycol dimethylacrylate (EGDMA) cross-linker was added to the PMM_{28} during synthesis in an attempt to retain all carboxylic acid groups on the inner membrane leaflet,[50] to "lock" the chains in place. EGDMA-crosslinked PMM_{28} were electroporated at 750 V in the presence of mixed valence iron solution as described above. TEM images without negative staining showed magnetopolymersomes similar to those shown in Fig. 4 and 5a but of a smaller average diameter (80 nm) (ESI 5†), but importantly, the outer halo was still present showing little difference between polymersomes pro-

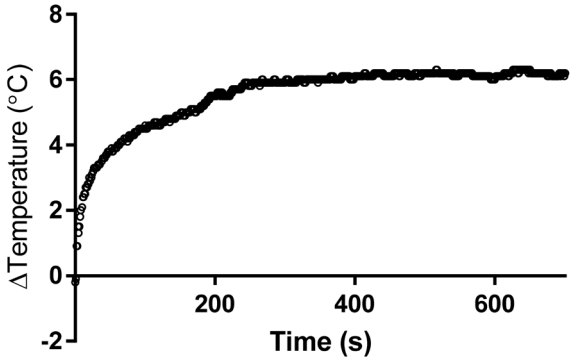

Fig. 6 Temperature increase *vs.* time curve obtained during magnetic hyperthermic heating of a 0.2% w/v aqueous dispersion of $PMM_{28}Fe$ polymersomes (0.11 mg ml^{-1} of iron). A temperature increase of 6 °C is observed over a period of 10 minutes (600 s).

duced with and without the EGDMA crosslinker. If anything there is less MNP precipitated in the core of the EGDMA crosslinked PMM_{28}. We can thus conclude flipping of the $PMPC_{28}$-$PHPMA_{400}$ block onto the outer surface post formation is not the dominant reason for surface iron oxide precipitation. Thus it is clear that either some of the carboxylic acid groups misorientation to the exterior during polymersome formation, or the precipitation on the surface is simply due to some NaOH leaking out during electroporation and is bound at the external membrane pore site.

Hyperthermic heating effect of $PMM_{28}Fe$ magnetopolymersomes

The biomedical hyperthermia treatment potential of $PMM_{28}Fe$ magnetopolymersomes was investigated. $PMM_{28}Fe$ were exposed to an alternating magnetic field to determine their potential for magnetic hyperthermia by assessing their heating power (over a 10 minutes period). A control of the blank PMM_{28} polymersome in PBS (ESI 6†) was subtracted from the final heating power of the magnetopolymersomes (Fig. 6). A temperature increase of 6 °C was observed over a 10 minutes period. A SAR value of 122 W g^{-1} and an ILP of 3.7 nHm^2 kg^{-1} was thus calculated. In principle, such localized heating can sensitize surrounding tissue towards a therapeutic payload that could be delivered within the same polymersomes.

Conclusions

In this work we have successfully designed and synthesized an asymmetric polymersomes with a selectively orientated smaller acidic block copolymer ($PMPC_{28}$-$PHPMA_{400}$) in the interior and a larger PEG_{113}-$PHPMA_{400}$ block copolymer forming the exterior of the vesicle to create a polymersome mimic of a magnetosome (PMM_{28}). Similar to our previous work producing magnetopolymersomes, we used electroporation to allow iron ion transport across the membrane and into the core of the vesicle to precipitate iron oxide. Unlike our previous work, here we have been successful in precipitating dense, magnetic, crystalline iron oxide within the core of the vesicle (closer to resembling a magnetosome) due to iron ion binding and iron-oxide nucleation capacity of the COO^- functional groups exposed on the inner leaflet in the core.

The iron oxide core of $PMM_{28}Fe$ is not a single crystal but an aggregation of 5.5 nm sized MNPs of high density in the centre, with discreet MNP being visible near the membrane.

The addition of the acidic nucleation sites have not only targeted the MNP precipitation into the core of PMM_{28} but has also lead to larger MNP within the magnetopolymersome. A small amount of exterior surface iron oxide precipitation is seen which was not reduced by cross-linking the PMM_{28} during formation.

Finally, $PMM_{28}Fe$ magnetopolymersomes were found to have advantageous properties with respect to potential future magnetic hyperthermia treatments, achieving a 6 °C heat increase in 10 minutes. In principle, such magnetite-loaded polymersomes can sensitize tissue for the *in vivo* delivery of a therapeutic payload or serve as a contrast agent for MRI diagnostic applications.[27] Furthermore, the use of polymersomes enable greater ability to design in multiple responsive functionalities for novel bioinspired smart nanomedical materials.

Conflicts of interest

There are no conflicts of interest to declare.

Acknowledgements

We would like to thank Mr Neil Bramall (Department of Chemistry, University of Sheffield) for collecting all ICP-ES data. Joseph Lovett is a Post doctoral research associate and Deborah Beattie is a PhD student both working for Prof. Steve Armes. We thank Steve for collaborating with us on this project: helping to supervise Masters student authors Catherine Dirk and Annie Sahota along with helpful advice and comments. We would like to thank Dr Andrea Rawlings for technical support, help and advice in the lab. We would also like to thank the EPSRC (grant no. EP/I032355/2) for funding this research.

References

1 J. L. Kirschvink, A. Kobayashi-Kirschvink and B. J. Woodford, Magnetite biomineralization in the human brain, *Proc. Natl. Acad. Sci. U. S. A.*, 1992, **89**, 7683–7687.
2 J. L. Kirschvink and J. W. Hagadorn, *10 A grand unified theory of biomineralization, The Biomineralisation of Nano- and Micro-Structures*, Wiley-VCH Verlag GmbH, Weinheim, Germany, 2000, pp. 139–150.
3 H. Skinner and A. Jahren, Biomineralization, *Treatise Geochem.*, 2003, **8**, 117–184.
4 S. Mann, *Biomineralization: Principles and Concepts in Bioinorganic Materials Chemistry*, 2001.

5 D. H. Nies, How iron is transported into magnetosomes, *Mol. Microbiol.*, 2011, **82**, 792–796.
6 A. Komeili, H. Vali, T. J. Beveridge and D. K. Newman, Magnetosome vesicles are present before magnetite formation, and MamA is required for their activation, *Proc. Natl. Acad. Sci. U. S. A.*, 2004, **101**, 3839.
7 S. Weiner and L. Addadi, Acidic macromolecules of mineralized tissues: The controllers of crystal formation, *Trends Biochem. Sci.*, 1991, **16**, 252–256.
8 J. Sodek, B. Ganss and M. D. McKee, Osteopontin, *Crit. Rev. Oral Biol. Med.*, 2000, **11**, 279–303.
9 W. Jiang, *et al.*, Chiral acidic amino acids induce chiral hierarchical structure in calcium carbonate, *Nat. Commun.*, 2017, **8**, 15066.
10 A. Arakaki, J. Webb and T. Matsunaga, A novel protein tightly bound to bacterial magnetic particles in Magnetospirillum magneticum strain AMB-1, *J. Biol. Chem.*, 2003, **278**, 8745–8750.
11 Y. Amemiya, A. Arakaki, S. S. Staniland, T. Tanaka and T. Matsunaga, Controlled formation of magnetite crystal by partial oxidation of ferrous hydroxide in the presence of recombinant magnetotactic bacterial protein Mms6, *Biomaterials*, 2007, **28**, 5381–5389.
12 S. S. Staniland and A. E. Rawlings, Crystallizing the function of the magnetosome membrane mineralization protein Mms6, *Biochem. Soc. Trans.*, 2016, **44**, 883–890.
13 S. M. Bird, A. E. Rawlings, J. M. Galloway and S. S. Staniland, Using a biomimetic membrane surface experiment to investigate the activity of the magnetite biomineralisation protein Mms6, *RSC Adv.*, 2016, **6**, 7356–7363.
14 S. Kashyap, T. J. Woehl, X. Liu, S. K. Mallapragada and T. Prozorov, Nucleation of Iron Oxide Nanoparticles Mediated by Mms6 Protein in Situ, *ACS Nano*, 2014, **8**, 9097–9106.
15 L. Wang, *et al.*, Self-Assembly and Biphasic Iron-Binding Characteristics of Mms6, A Bacterial Protein That Promotes the Formation of Superparamagnetic Magnetite Nanoparticles of Uniform Size and Shape, *Biomacromolecules*, 2012, **13**, 98–105.
16 A. E. Rawlings, *et al.*, Ferrous iron key to Mms6 magnetite biomineralisation: A mechanistic study to understand magnetite formation using pH titration and NMR, *Chem. – Eur. J.*, 2016, **22**, 7885–7894.
17 D. Murat, *et al.*, The magnetosome membrane protein, MmsF, is a major regulator of magnetite biomineralization in Magnetospirillum magneticum AMB-1, *Mol. Microbiol.*, 2012, **85**, 684–699.
18 H. Nudelman and R. Zarivach, Structure prediction of magnetosome-associated proteins, *Front. Microbiol.*, 2014, **5**, 9.
19 S. M. Janib, A. S. Moses and J. A. MacKay, Imaging and drug delivery using theranostic nanoparticles, *Adv. Drug Delivery Rev.*, 2010, **62**, 1052–1063.
20 L. Guan, L. Rizzello and G. Battaglia, Polymersomes and their applications in cancer delivery and therapy, *Nanomedicine*, 2015, **10**, 2757–2780.
21 D. Schmaljohann, Thermo- and pH-responsive polymers in drug delivery, *Adv. Drug Delivery Rev.*, 2006, **58**, 1655–1670.
22 M. Kallumadil, *et al.*, Suitability of commercial colloids for magnetic hyperthermia, *J. Magn. Magn. Mater.*, 2009, **321**, 1509–1513.
23 R. Hergt, *et al.*, Magnetic properties of bacterial magnetosomes as potential diagnostic and therapeutic tools, *J. Magn. Magn. Mater.*, 2005, **293**, 80–86.
24 A. Plan Sangnier, *et al.*, Targeted thermal therapy with genetically engineered magnetite magnetosomes@RGD: Photothermia is far more efficient than magnetic hyperthermia, *J. Controlled Release*, 2018, **279**, 271–281.
25 R. Hergt, S. Dutz, R. Müller and M. Zeisberger, Magnetic particle hyperthermia: nanoparticle magnetism and materials development for cancer therapy, *J. Phys.: Condens. Matter*, 2006, **18**, S2919–S2934.
26 R. Ludwig, *et al.*, Structural properties of magnetic nanoparticles determine their heating behavior - an estimation of the in vivo heating potential, *Nanoscale Res. Lett.*, 2014, **9**, 602.
27 Q. A. Pankhurst, J. Connolly, S. K. Jones and J. Dobson, Applications of magnetic nanoparticles in biomedicine, *J. Phys. D: Appl. Phys.*, 2003, **36**, R167–R181.
28 C. S. S. R. Kumar and F. Mohammad, Magnetic nanomaterials for hyperthermia-based therapy and controlled drug delivery, *Adv. Drug Delivery Rev.*, 2011, **63**(9), 789–808.
29 J. Bain, *et al.*, In situ formation of magnetopolymersomes via electroporation for MRI, *Sci. Rep.*, 2015, **5**, 14311.
30 J. Bain, M. Berry, C. Dirks and S. Staniland, Synthesis of ABA Tri-Block Co-Polymer Magnetopolymersomes via Electroporation for Potential Medical Application, *Polymers*, 2015, **7**, 1529.
31 J. C. Weaver, Electroporation: a general phenomenon for manipulating cells and tissues, *J. Cell. Biochem.*, 1993, **51**, 426–435.
32 J. Gehl, Electroporation: theory and methods, perspectives for drug delivery, gene therapy and research, *Acta Physiol. Scand.*, 2003, **177**, 437–447.
33 J. M. Escoffre, *et al.*, What is (still not) known of the mechanism by which electroporation mediates gene transfer and expression in cells and tissues, *Mol. Biotechnol.*, 2009, **41**, 286–295.
34 D. P. Tieleman, The molecular basis of electroporation, *BMC Biochem.*, 2004, **5**, 10.
35 L. Wang, *et al.*, Encapsulation of Biomacromolecules within Polymersomes by Electroporation, *Angew. Chem., Int. Ed.*, 2012, **51**, 11122–11125.
36 J. C. Weaver and Y. A. Chizmadzhev, Theory of electroporation: a review, *Bioelectrochem. Bioenerg.*, 1996, **41**, 135–160.
37 Y. Ning, *et al.* Incorporating Diblock Copolymer Nanoparticles into Calcite Crystals: Do Anionic Carboxylate Groups Alone Ensure Efficient Occlusion?, *ACS Macro Lett.*, 2016, **5**, 311–315.
38 A. Blanazs, N. J. Warren, A. L. Lewis, S. P. Armes and A. J. Ryan, Self-assembly of double hydrophilic block copolymers in concentrated aqueous solution, *Soft Matter*, 2011, **7**, 6399–6403.

39 D. E. Discher and A. Eisenberg, Polymer vesicles, *Science*, 2002, **297**, 967–973.
40 M. Antonietti and S. Förster, Vesicles and Liposomes: A Self-Assembly Principle Beyond Lipids, *Adv. Mater.*, 2003, **15**, 1323–1333.
41 S. Jain and F. S. Bates, On the Origins of Morphological Complexity in Block Copolymer Surfactants, *Science*, 2003, **300**, 460–464.
42 L. Zhang and A. Eisenberg, Formation of crew-cut aggregates of various morphologies from amphiphilic block copolymers in solution, *Polym. Adv. Technol.*, 1998, **9**, 677–699.
43 A. Blanazs, S. P. Armes and A. J. Ryan, Self-Assembled Block Copolymer Aggregates: From Micelles to Vesicles and their Biological Applications, *Macromol. Rapid Commun.*, 2009, **30**, 267–277.
44 W. Zhang, F. D'Agosto, O. Boyron, J. Rieger and B. Charleux, Toward a Better Understanding of the Parameters that Lead to the Formation of Nonspherical Polystyrene Particles via RAFT-Mediated One-Pot Aqueous Emulsion Polymerization, *Macromolecules*, 2012, **45**, 4075–4084.
45 N. J. Warren and S. P. Armes, Polymerization-Induced Self-Assembly of Block Copolymer Nano-objects via RAFT Aqueous Dispersion Polymerization, *J. Am. Chem. Soc.*, 2014, **136**, 10174–10185.
46 S. L. Canning, G. N. Smith and S. P. Armes, A Critical Appraisal of RAFT-Mediated Polymerization-Induced Self-Assembly, *Macromolecules*, 2016, **49**, 1985–2001.
47 S. Sugihara, A. Blanazs, S. P. Armes, A. J. Ryan and A. L. Lewis, Aqueous Dispersion Polymerization: A New Paradigm for in Situ Block Copolymer Self-Assembly in Concentrated Solution, *J. Am. Chem. Soc.*, 2011, **133**, 15707–15713.
48 C. Gonzato, *et al.* Rational Synthesis of Low-Polydispersity Block Copolymer Vesicles in Concentrated Solution via Polymerization-Induced Self-Assembly, *J. Am. Chem. Soc.*, 2014, **136**, 11100–11106.
49 J. R. Lovett, N. J. Warren, L. P. Ratcliffe, M. K. Kocik and S. P. Armes, pH-responsive non-ionic diblock copolymers: ionization of carboxylic acid end-groups induces an order-order morphological transition, *Angew. Chem., Int. Ed.*, 2015, **54**, 1279–1283.
50 P. Chambon, A. Blanazs, G. Battaglia and S. P. Armes, Facile Synthesis of Methacrylic ABC Triblock Copolymer Vesicles by RAFT Aqueous Dispersion Polymerization, *Macromolecules*, 2012, **45**, 5081–5090.
51 R. R. Wildeboer, P. Southern and Q. A. Pankhurst, On the reliable measurement of specific absorption rates and intrinsic loss parameters in magnetic hyperthermia materials, *J. Phys. D: Appl. Phys.*, 2014, **47**, 495003.